Practical Mechanisms to Realize Smooth Transitions for Unconventional Multi-sensor Integrated Kinematic Positioning and Navigation

Fei Yu, Minghong Zhu*, Shu Xiao*, and Jianguo Wang

***Abstract*—Conventionally, the Kalman filter on the basis of integration mechanization, such as GPS-aided inertial integrated navigation system, has been commonly built up using error states and error measurements. In order to accurately reflect the evolution of the real state for a moving vehicle, we adopted an unconventional KF that directly estimated navigational parameters instead of the error states, in which a kinematic trajectory model as the main part of KF system model was deployed and measurement updates for all sensor data inclusive of the ones from IMUs were directly performed. To best describe the trajectory instead of applying the most complex model throughout, this research proposed relevant practical mechanisms for linear motion and circular motion to realize smooth transitions between alternative kinematic models. Experiments and simulations were tested to show the practicability of the proposed practical approach.**

***Index Terms*—smooth transitions, unconventional, multi-sensor, integration, kinematic.**

I. Introduction

As competitive consumer markets bring a great price reduction of mobile navigation devices, low-cost IMUs have recently received more and more attention. But low accuracy is one of the biggest bottlenecks in development of low-cost IMUs. A popular approach to design sensors for systems requiring better performance than the one with a single low-cost IMU may offer, is to fuse the measurements of multiple low-cost IMUs to achieve advantage complementarity. This "wisdom of the crowd" design approach also has, in addition to the increased measurement performance, the benefit of making it possible to detect and isolate sensor failures, thereby increasing the reliability and integrity of the sensor system [1].

The key of combining multiple sensors for accuracy improvement lies in rate signal modeling and the optimal filter design [2]. In this respect, researchers have done a lot of work. However, in most work from the view of algorithm design, the core error-state-based system equations still remain the same as in the conventional strategy built upon the inertial navigation mechanization [3], [4]. The conventional integration strategy driven by the *a priori* error model of inertial sensor could become problematic in the case of low-cost MEMS IMUs as their time-variant noise model could be highly sensitive to the temperature [5] and the dynamic excitations [6]. A significant reformation in the integration strategy for low-cost IMU-based multi-sensor integrated navigation systems is quite demanded considering one may not be able to reach an innovative and cost-effective breakthrough if one still remains in the traditional rut.

Wang et al. [2015] and Qian et al. [2016] already developed an unconventional KF that could directly estimate navigational parameters instead of the error states, in which a kinematic trajectory model as the main part of KF system model was deployed and measurement updates for all sensor data inclusive of the ones from IMUs were directly performed [7], [8], [9]. This design enables the direct use of the IMUs' raw outputs (specific forces and angular rates) instead of applying them to the free inertial navigation calculation through the conventional inertial integration mechanization. Besides, to visually provide the dynamic process of system navigation parameters, and accurately reflect the evolution of real state in kinematic navigation, direct Kalman filter (DKF) deserves consideration. The reason why DKF is not widely discussed previously is not the method itself, but most system models are serious nonlinear so that DKF is inapplicable. Therefore, it is a bright proposal that the three-dimensional (3D) kinematic trajectory model is deployed as system model in KF. However, there are certain defects existing in the 3D kinematic trajectory model proposed before, in that the less complex kinematic model cannot realize smooth transitions between alternative kinematic models. A moving platform is certain to experience different motions from time to time in a mission. One should avoid employing the most complex kinematic model as the core system model throughout. A proper model will not only avoid getting over parametrization involved and also be able to properly model the system maneuvers.

This research applied the above mentioned novel multi-sensor integration strategy to integrate GPS receiver and multiple IMUs. The obvious advantage how the low-cost IMU arrays are fused here is to enable the direct measurement updates for individual IMUs and model their systematic errors separately in KF. In view of the problem of smooth transitions, this research developed practical mechanisms to realize smooth transitions between different motion statuses. This is to best describe the trajectory instead of applying the most complex model throughout. Four basic kinematic models (uniform linear motion, uniformly accelerated linear motion, uniform circular motion and non-uniform circular motion) with their associated process noise factors will be

Manuscript received October 13, 2017; revised May 28, 2018. This work was supported by the National Natural Science Foundation of China under Grant No. 51679047.

F. Yu is with the College of Automation, Harbin Engineering University, Harbin, P.R.China.

M. H. Zhu (Corresponding author) is with the College of Automation, Harbin Engineering University, Harbin, P.R.China (e-mail: zhuminghong@hrbeu.edu.cn).

S. Xiao (Corresponding author) is with the College of Automation, Harbin Engineering University, Harbin, P.R.China (e-mail: xsh617@126.com).

J. G. Wang is with the Department of Earth and Space Science and Engineering, York University, Toronto, Canada.

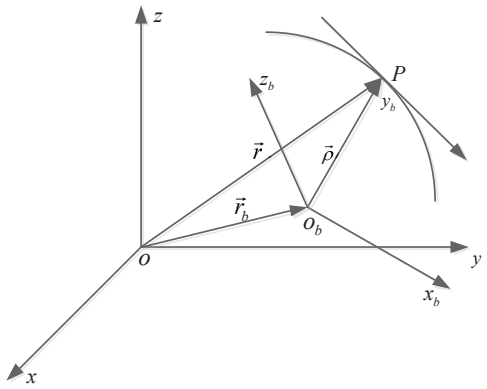

Fig. 1. The Coordinate Systems

considered and explicitly specified. Then, practical mechanisms will be developed to realize switches between different kinematic models by utilizing the changes of linear and circular velocities and accelerations together with the changes of system attitudes. The main challenge is how to determine the detection rules for significant system maneuvers under the consideration of not only their magnitudes, but also their accuracies or resolutions associated with specific system dynamics.

In the following, the 3D kinematic trajectory model for a rigid body is discussed in Section II. The formulation of the unconventional multi-sensor Kalman filter is described in Section III. Section IV presents the practical mechanisms (PMs) to realize smooth transitions. Section V provides the simulation results to validate the proposed PMs for unconventional multi-sensor integrated kinematic positioning and navigation. Conclusions are given in Section VI.

II. Three-Dimensional Kinematic Trajectory Model

The motion of a rigid body can be described through the kinematics without concerning the force as the causes for different motion types. Appropriate coordinate frames are needed to mathematically represent the position, velocity and acceleration of a mechanical system. Two reference frames, which are moving to each other, are used as in Fig. 1. One of the frames is called as space-fixed system $oxyz((S)$, the other one is as the moved one $o_bx_by_bz_b(S_b)$, S_b is also called the body frame.

The position vector of a point P will be uniquely represented through a time-dependent position vector $\tilde{\mathbf{r}}$ with the help of three unit vectors $\vec{i}, \vec{j}, \vec{k}$ along three axes x, y, z in the space-fixed frame:

$$\tilde{\mathbf{r}} = x\tilde{\mathbf{i}} + y\tilde{\mathbf{j}} + z\tilde{\mathbf{k}} \tag{1}$$

In components, the motion of the point at a time instant t relative to a start time t_0 can be given by

$$x(t) = x(t_0)+\dot{x}(t_0)(t-t_0)+\tfrac{1}{2}\ddot{x}(t_0)(t-t_0)^2+\tfrac{1}{6}\dddot{x}(t_0)(t-t_0)^3+\cdots \tag{2}$$

$$y(t) = y(t_0)+\dot{y}(t_0)(t-t_0)+\tfrac{1}{2}\ddot{y}(t_0)(t-t_0)^2+\tfrac{1}{6}\dddot{y}(t_0)(t-t_0)^3+\cdots \tag{3}$$

$$z(t) = z(t_0)+\dot{z}(t_0)(t-t_0)+\tfrac{1}{2}\ddot{z}(t_0)(t-t_0)^2+\tfrac{1}{6}\dddot{z}(t_0)(t-t_0)^3+\cdots \tag{4}$$

wherein, $\dot{x}, \ddot{x}, \dddot{x},\ \dot{y}, \ddot{y}, \dddot{y},\ \dot{z}, \ddot{z}, \dddot{z}, ...$ are the first to third derivatives of x, y, z with respect to the time. In order to require as less items as possible, the time interval $(t - t_0)$ must be as short as possible. Let $\tilde{\mathbf{r}}_0$ be the position vector of the origin O_b and $\tilde{\rho}$ and $\tilde{\rho}_\mathbf{b}$ be the relative position vector of point P from O_b and the same vector in S_b, then

$$\tilde{\mathbf{r}}(t) = \tilde{\mathbf{r}}_0(t) + \tilde{\rho}(t) = \tilde{\mathbf{r}}_0(t) + \mathbf{D}^T(t)\tilde{\rho}_b(t) \tag{5}$$

wherein, $\mathbf{D}(t)$ is the instantaneous rotation matrix from S to S_b. From (5), the velocity, acceleration and jerk vectors can be derived successively. The angular motion is coupled with $\mathbf{D}(t)$.

With regard to a moving rigid body, the basic trajectory parameters of interest are the relative parameters in the local navigation frame (S_n), such as position vector $\mathbf{r}^n_{nb}$ of the IMU center, the velocity vector $\mathbf{v}^n_{nb}$, the acceleration vector $\mathbf{a}^n_{nb}$ and even the jerk vector $\mathbf{j}^n_{nb}$. In principle, $\mathbf{v}^n_{nb}$ is the derivative of $\mathbf{r}^n_{nb}$, which is also transformed from its counterpart velocity vector $\mathbf{v}^b_{nb}$ in S_b. Similarly, $\mathbf{a}^n_{nb}$ and $\mathbf{j}^n_{nb}$ are the derivatives of $\mathbf{v}^n_{nb}$ and $\mathbf{a}^n_{nb}$.

For practical applications, position vector $\mathbf{r}$ of a moving vehicle is discussed frequently in earth-fixed coordinate frame (S_e), so position vector $\mathbf{r}$ in S_e is calculated here. One step location update from point A to point B within a small enough time interval Δt is given as an example.

Firstly, the local coordinate increment $\Delta\mathbf{r}_n$ from point A to point B with a zero initialization in S_n is described in (6).

$$\Delta\mathbf{r}_n = \Delta t\mathbf{C}^n_{b(A)}\mathbf{v}^b_{nb(A)}+\frac{\Delta t^2}{2}\mathbf{C}^n_{b(A)}\mathbf{a}^b_{nb(A)}+\frac{\Delta t^3}{6}\mathbf{C}^n_{b(A)}\mathbf{j}^b_{nb(A)} \tag{6}$$

wherein, $\mathbf{C}^n_b$ is the direction cosine matrix (DCM) from S_b to S_n. The subscript A represents time A.

Secondly, the local coordinate increment is transformed from S_n to S_e through the position cosine matrix $\mathbf{C}^e_{n(A)}$ at point A in (7).

$$\Delta\mathbf{r}_e = \mathbf{C}^e_{n(A)}\Delta\mathbf{r}_n \tag{7}$$

Finally, substituting (6) into (7), position vector $\mathbf{r}$ can be listed in (8).

$$\mathbf{r}^B_A = \mathbf{r}_A + \Delta\mathbf{r}_e = \mathbf{r}_A + \mathbf{C}^e_{n(A)}\Delta\mathbf{r}_n = \mathbf{r}_A + \mathbf{C}^e_{n(A)}\cdot (\Delta t\mathbf{C}^n_{b(A)}\mathbf{v}^b_{nb(A)} + \tfrac{\Delta t^2}{2}\mathbf{C}^n_{b(A)}\mathbf{a}^b_{nb(A)} + \tfrac{\Delta t^3}{6}\mathbf{C}^n_{b(A)}\mathbf{j}^b_{nb(A)}) \tag{8}$$

By the rule of the vector dynamics, the rest of trajectory parameters are directly given as:

$$\dot{\mathbf{r}}^n_{nb} = \mathbf{v}^n_{nb} = \mathbf{C}^n_b\mathbf{v}^b_{nb} \tag{9}$$

$$\dot{\mathbf{v}}^n_{nb} = \mathbf{a}^n_{nb} = \mathbf{C}^n_b[\omega^b_{nb}\times]\mathbf{v}^b_{nb} + \mathbf{C}^n_b(\ \dot{\mathbf{v}}^b_{nbx}\quad \dot{\mathbf{v}}^b_{nby}\quad \dot{\mathbf{v}}^b_{nbz}\ )^T = \mathbf{C}^n_b\mathbf{a}^b_{nb} \tag{10}$$

$$\dot{\mathbf{a}}^n_{nb} = \mathbf{j}^n_{nb} = \mathbf{C}^n_b[\omega^b_{nb}\times]\mathbf{a}^b_{nb} + \mathbf{C}^n_b(\ \dot{\mathbf{a}}^b_{nbx}\quad \dot{\mathbf{a}}^b_{nby}\quad \dot{\mathbf{a}}^b_{nbz}\ )^T = \mathbf{C}^n_b\mathbf{j}^b_{nb} \tag{11}$$

wherein, $\mathbf{r}^n_{nb}, \mathbf{v}^n_{nb}, \mathbf{a}^n_{nb}, \mathbf{j}^n_{nb}, \omega^n_{nb}$ are the position, velocity, acceleration, jerk and angular rate vectors in S_n respectively. $\mathbf{v}^b_{nb}, \mathbf{a}^b_{nb}, \mathbf{j}^b_{nb}$ are the velocity, acceleration and jerk vectors in S_b. $\mathbf{C}^n_b$ is the DCM.

III. Formulation of The Unconventional Kalman Filter

In this research, the KF system model consists of three parts: 1) the 3D kinematic trajectory; 2) the attitudes; 3) the

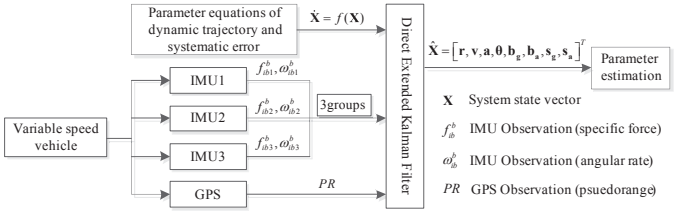

Fig. 2. Unconventional Integration Mechanism

angular rate. The first part is already discussed in Section II. Please refer to [7] and [8] for the attitude model and angular rate model.

Without loss of generality, the state vector and measurement vector should be provided for the system Kalman filter. For this research, the whole-value-state which describes the vehicle's kinetic characteristic is one part of the state vector. The systematic errors of multiple IMUs are individually modeled in the navigation Kalman filter, instead of being a group of the commonly shared states for all of the IMUs because the assumption of the common-mode errors of different sensors of the same design is unreasonable. Therefore, the systematic-error of multi-IMU is the other part of the state vector. As to the measurement vector, the measurements of IMUs and GPS are considered, and all measurements are the raw observables from IMUs and GPS. Fig. 2 shows the unconventional integration mechanism. In this paper, one GPS receiver and three low-cost IMUs are integrated as a multi-sensor system to be processed.

A. The State Vector of Kalman Filter

The state vector of the being structured multi-sensor integration Kalman filter in this manuscript consists of 51 components as follows

$$\mathbf{X}_{51\times1} = \left[\begin{array}{c} \mathbf{r}^T, (\mathbf{v}^b_{nb})^T, (\mathbf{a}^b_{nb})^T, \theta^T, (\omega^b_{nb})^T, \mathbf{b}^T_{g1}, \mathbf{b}^T_{g2}, \\ \mathbf{b}^T_{g3}, \mathbf{b}^T_{a1}, \mathbf{b}^T_{a2}, \mathbf{b}^T_{a3}, \mathbf{s}^T_{g1}, \mathbf{s}^T_{g2}, \mathbf{s}^T_{g3}, \mathbf{s}^T_{a1}, \mathbf{s}^T_{a2}, \mathbf{s}^T_{a3} \end{array}\right]^T$$

with $\mathbf{r} = (\ X \quad Y \quad Z\ )^T$, $\mathbf{v}^b_{nb} = (\ v^b_{nbx} \quad v^b_{nby} \quad v^b_{nbz}\ )^T$, $\mathbf{a}^b_{nb} = (\ a^b_{nbx} \quad a^b_{nby} \quad a^b_{nbz}\ )^T$, $\theta = (\ P \quad \gamma \quad \psi\ )^T$, $\omega^b_{nb} = (\ \omega^b_{nbx} \quad \omega^b_{nby} \quad \omega^b_{nbz}\ )^T$, which are the position in earth-fixed coordinate frame (WGS84), body velocity, body acceleration, the attitude and body angular rate vectors. With $\mathbf{b}_{g1} = (\ b_{g1x} \quad b_{g1y} \quad b_{g1z}\ )^T$, $\mathbf{b}_{g2} = (\ b_{g2x} \quad b_{g2y} \quad b_{g2z}\ )^T$, $\mathbf{b}_{g3} = (\ b_{g3x} \quad b_{g3y} \quad b_{g3z}\ )^T$, $\mathbf{b}_{a1} = (\ b_{a1x} \quad b_{a1y} \quad b_{a1z}\ )^T$, $\mathbf{b}_{a2} = (\ b_{a2x} \quad b_{a2y} \quad b_{a2z}\ )^T$, $\mathbf{b}_{a3} = (\ b_{a3x} \quad b_{a3y} \quad b_{a3z}\ )^T$, $\mathbf{s}_{g1} = (\ s_{g1x} \quad s_{g1y} \quad s_{g1z}\ )^T$, $\mathbf{s}_{g2} = (\ s_{g2x} \quad s_{g2y} \quad s_{g2z}\ )^T$, $\mathbf{s}_{g3} = (\ s_{g3x} \quad s_{g3y} \quad s_{g3z}\ )^T$, $\mathbf{s}_{a1} = (\ s_{a1x} \quad s_{a1y} \quad s_{a1z}\ )^T$, $\mathbf{s}_{a2} = (\ s_{a2x} \quad s_{a2y} \quad s_{a2z}\ )^T$, $\mathbf{s}_{a3} = (\ s_{a3x} \quad s_{a3y} \quad s_{a3z}\ )^T$, which are gyroscope bias, accelerometer bias, gyroscope scale factor error and accelerometer scale factor error vectors, respectively. Moreover, subscripts 1, 2 and 3 represent serial numbers of the three IMUs.

B. Discrete System Model

According to the differential equations in Section II, the discrete system equations for Kalman filter can be summarized after the omission of the high order terms in Taylor series expansion. The system discrete model can be given as follows:

$$\begin{aligned}\mathbf{r}_{k+1} = \mathbf{r}_k + \mathbf{C}^e_{n(k)}(&\Delta t \mathbf{C}^n_{b(k)}\mathbf{v}^b_{nb(k)} \\ &+\tfrac{\Delta t^2}{2}\mathbf{C}^n_{b(k)}\mathbf{a}^b_{nb(k)} + \tfrac{\Delta t^3}{6}\mathbf{C}^n_{b(k)}\mathbf{j}^b_{nb(k)})\end{aligned} \tag{12}$$

$$\begin{aligned}\mathbf{v}^b_{nb(k+1)} = &\left[\mathbf{I}_{3\times3} - \Delta t\left[\omega^b_{nb(k)}\times\right] + \tfrac{\Delta t^2}{2}\left[\omega^b_{nb(k)}\times\right]^2\right]\mathbf{v}^b_{nb(k)} \\ &+\left[\Delta t\mathbf{I}_{3\times3} - \Delta t^2\left[\omega^b_{nb(k)}\times\right]\right]\mathbf{a}^b_{nb(k)} \\ &+\tfrac{\Delta t^2}{2}\left[\mathbf{v}^b_{nb(k)}\times\right]\dot{\omega}^b_{nb(k)} + \tfrac{\Delta t^2}{2}\mathbf{j}^b_{nb(k)}\end{aligned} \tag{13}$$

$$\begin{aligned}\mathbf{a}^b_{nb(k+1)} = &\left[\mathbf{I}_{3\times3} - \Delta t\left[\omega^b_{nb(k)}\times\right] + \tfrac{\Delta t^2}{2}\left[\omega^b_{nb(k)}\times\right]^2\right]\mathbf{a}^b_{nb(k)} \\ &+\tfrac{\Delta t^2}{2}\left[\mathbf{a}^b_{nb(k)}\times\right]\dot{\omega}^b_{nb(k)} + \Delta t\mathbf{j}^b_{nb(k)}\end{aligned} \tag{14}$$

$$\theta_{(k+1)} = \theta_{(k)} + \Delta t\mathbf{C}_{3\times3}\omega^b_{nb(k)} + \frac{\Delta t^2}{2}\mathbf{C}_{3\times3}\dot{\omega}^b_{nb} \tag{15}$$

$$\omega^b_{nbx(k+1)} = e^{-\Delta t/T_x}\omega^b_{nbx(k)} + w_{\omega x} \tag{16}$$

$$\omega^b_{nby(k+1)} = e^{-\Delta t/T_y}\omega^b_{nby(k)} + w_{\omega y} \tag{17}$$

$$\omega^b_{nbz(k+1)} = e^{-\Delta t/T_z}\omega^b_{nbz(k)} + (1-e^{-\Delta t/T_z})\omega^b_{nbz(k-1)} + w_{\omega z} \tag{18}$$

$$\mathbf{b}_{g1}(k+1) = \mathbf{b}_{g1}(k) + \mathbf{w}_{b_{g1}} \tag{19}$$

$$\mathbf{b}_{g2}(k+1) = \mathbf{b}_{g2}(k) + \mathbf{w}_{b_{g2}} \tag{20}$$

$$\mathbf{b}_{g3}(k+1) = \mathbf{b}_{g3}(k) + \mathbf{w}_{b_{g3}} \tag{21}$$

$$\mathbf{b}_{a1}(k+1) = \mathbf{b}_{a1}(k) + \mathbf{w}_{b_{a1}} \tag{22}$$

$$\mathbf{b}_{a2}(k+1) = \mathbf{b}_{a2}(k) + \mathbf{w}_{b_{a2}} \tag{23}$$

$$\mathbf{b}_{a3}(k+1) = \mathbf{b}_{a3}(k) + \mathbf{w}_{b_{a3}} \tag{24}$$

$$\mathbf{s}_{g1}(k+1) = \mathbf{s}_{g1}(k) + \mathbf{w}_{s_{g1}} \tag{25}$$

$$\mathbf{s}_{g2}(k+1) = \mathbf{s}_{g2}(k) + \mathbf{w}_{s_{g2}} \tag{26}$$

$$\mathbf{s}_{g3}(k+1) = \mathbf{s}_{g3}(k) + \mathbf{w}_{s_{g3}} \tag{27}$$

$$\mathbf{s}_{a1}(k+1) = \mathbf{s}_{a1}(k) + \mathbf{w}_{s_{a1}} \tag{28}$$

$$\mathbf{s}_{a2}(k+1) = \mathbf{s}_{a2}(k) + \mathbf{w}_{s_{a2}} \tag{29}$$

$$\mathbf{s}_{a3}(k+1) = \mathbf{s}_{a3}(k) + \mathbf{w}_{s_{a3}} \tag{30}$$

where $\Delta t = t_{k+1} - t_k$ is the time interval. $\mathbf{C}^n_b$ is the DCM. T_x, T_y, T_z are the time correlation coefficients of the first order Markov model. $w_{\omega x}, w_{\omega y}, w_{\omega z}$ are three independent white noise components for the angular rates. w_{bg}, w_{sg}, w_{ba} and w_{sa} are the white noise vectors for the biases and scale factor errors of gyroscopes and accelerometers, and subscripts 1, 2 and 3 represent serial numbers of the three IMUs. $\mathbf{j}^b_{nb}$ is the body jerk vector as process noise for the position, velocity and acceleration vectors. $\dot{\omega}^b_{nb}$ is the derivation of angular rate vector as the process noise for velocity, acceleration and attitude vectors. $\mathbf{C}_{3\times3}$ is the coefficient matrix as

$$\mathbf{C}_{3\times3} = \left[\begin{array}{ccc} \cos\gamma & 0 & \sin\gamma \\ \sin\gamma\tan P & 1 & -\cos\gamma\tan P \\ \sin\gamma\sec P & 0 & -\cos\gamma\sec P \end{array}\right]$$

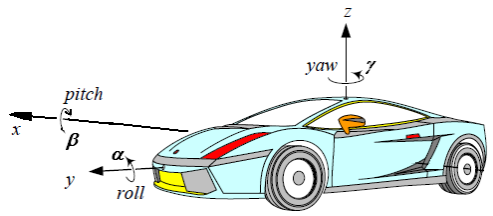

(a) Vehicle's General View

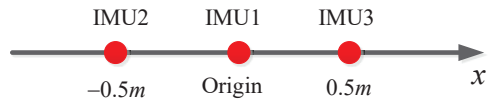

(b) Partial Enlarged Details for Internal Structure

Fig. 3. Structure Schematic of IMUs

$\mathbf{C}_n^e$ is position cosine matrix as follows, so its elements can be acquired through the position vector $\mathbf{r}$ in S_e.

$$\mathbf{C}_n^e = \begin{bmatrix} -\sin\lambda & -\sin\varphi\cos\lambda & \cos\varphi\cos\lambda \\ \cos\lambda & -\sin\varphi\sin\lambda & \cos\varphi\sin\lambda \\ 0 & \cos\varphi & \sin\varphi \end{bmatrix}$$

wherein, λ and φ are longitude and latitude respectively, and calculated by coordinate components (X, Y, Z) of the position vector $\mathbf{r}$ in S_e.

C. IMU Measurement Model

In general, the raw outputs of an IMU consist of three angular rates from three orthogonal gyroscopes and three specific forces from three accelerometers. Since there are three IMUs in this integration system, three groups of measurement equations need to be derived. Three IMUs are placed as shown in Fig. 3, of which Fig. 3(a) is the vehicle's general view and Fig. 3(b) is the partial enlarged details for internal structure.

Meanwhile, depending on specific application, the measurement equations for low-cost IMUs can be simplified [10], [11]. Considering each IMU can not be located at the same point on the body, the different measurements from IMUs must be transformed to the same reference frame in order to perform the fusion algorithm [12], [13]. Here the core IMU is chosen as reference. Three groups of angular rate measurement equations and three groups of specific force measurement equations are derived according to the specific structure as follows:

$$\omega_{ib-imu1}^b = (\mathbf{I} + \mathbf{S}_{g1})\omega_{nb}^b + \mathbf{b}_{g1} + \mathbf{\Delta}_{g1} \quad (31)$$

$$\omega_{ib-imu2}^b = (\mathbf{I} + \mathbf{S}_{g2})\omega_{nb}^b + \mathbf{b}_{g2} + \mathbf{\Delta}_{g2} \quad (32)$$

$$\omega_{ib-imu3}^b = (\mathbf{I} + \mathbf{S}_{g3})\omega_{nb}^b + \mathbf{b}_{g3} + \mathbf{\Delta}_{g3} \quad (33)$$

$$\mathbf{f}_{ib-imu1}^b = (\mathbf{I} + \mathbf{S}_{a1})(\mathbf{a}_{nb}^b - \mathbf{C}_n^b\mathbf{g}^n) + \mathbf{b}_{a1} + \mathbf{\Delta}_{a1} \quad (34)$$

$$\mathbf{f}_{ib-imu2}^b = (\mathbf{I}+\mathbf{S}_{a2})(\mathbf{a}_{nb}^b-\mathbf{C}_n^b\mathbf{g}^n)+\omega_{ib}^b\times(\omega_{ib}^b\times\mathbf{r}_2)+\mathbf{b}_{a2}+\mathbf{\Delta}_{a2} \quad (35)$$

$$\mathbf{f}_{ib-imu3}^b = (\mathbf{I}+\mathbf{S}_{a3})(\mathbf{a}_{nb}^b-\mathbf{C}_n^b\mathbf{g}^n)+\omega_{ib}^b\times(\omega_{ib}^b\times\mathbf{r}_3)+\mathbf{b}_{a3}+\mathbf{\Delta}_{a3} \quad (36)$$

wherein, $\mathbf{g}^n$ is the local gravity vector in S_n. $\omega_{nb}^b, \mathbf{a}_{nb}^b$ are the rotation rate vector and the acceleration vector of S_b with respect to S_n. $\mathbf{b}_g, \mathbf{b}_a$ are the same meanings as mentioned in Subsection III-A. $\mathbf{S}_g, \mathbf{S}_a$ are the 3×3 scale factor error matrices for gyroscopes and accelerometers. $\mathbf{\Delta}_g, \mathbf{\Delta}_a$ are the Gaussian white noise vectors for angular rate and specific force vectors. The lever arm parameters of the other two IMUs with respect to the core one $\mathbf{r}_2 = [-0.5, 0, 0]^T$ and $\mathbf{r}_3 = [0.5, 0, 0]^T$.

D. GPS Measurement Model

In this research, not only the IMUs' raw outputs, but also the GPS's raw outputs are directly used during measurement updates. As another sensor different from low-cost IMUs but the same status in this system, GPS may offer two kinds of raw outputs, pseudorange and carrier phase. For this specific application, only pseudorange is utilized to complete system navigation. The generic observation equation [14], [15] for the pseudorange PR_A^j from receiver A to satellite j is

$$PR_A^j = \rho_A^j + c(\delta t_A - \delta t^j) + d_{A-trop}^j + d_{A-ion}^j + \varepsilon_{PR_A^j} \quad (37)$$

wherein, $j = 1, 2, \cdots, n$ indicates the $j-th$ satellite. ρ_A^j is the distance between receiver A and satellite j. c is the speed of light. $\delta t_A, \delta t^j$ are the receiver clock error and satellite clock error. $d_{A-trop}^j, d_{A-ion}^j$ are the tropospheric delay and ionospheric delay. $\varepsilon_{PR_A^j}$ is the random noise.

E. Kalman Filter Under the Unconventional Integration Strategy

Straightforward, the extended Kalman filter (EKF) is further constructed based on the system model proposed above. The state equations (12) - (30) and measurement equations (31) - (37) are respectively generalized by the discrete nonlinear system model as follows

$$\mathbf{X}_{k+1} = f(\mathbf{X}_k) + \mathbf{\Gamma}_k\mathbf{w}_k \quad (38)$$

$$\mathbf{Z}_k = h(\mathbf{X}_k) + \mathbf{v}_k \quad (39)$$

wherein, $\mathbf{X}_k$ is the state vector as defined in Subsection III-A.

$$\mathbf{w}_k = \begin{bmatrix} (\mathbf{j}_{nb}^b)^T, (\dot{\omega}_{nb}^b)^T, w_x, w_y, w_z, (\mathbf{w}_{bg1})^T, (\mathbf{w}_{bg2})^T, \\ (\mathbf{w}_{bg3})^T, (\mathbf{w}_{ba1})^T, (\mathbf{w}_{ba2})^T, (\mathbf{w}_{ba3})^T, (\mathbf{w}_{sg1})^T, \\ (\mathbf{w}_{sg2})^T, (\mathbf{w}_{sg3})^T, (\mathbf{w}_{sa1})^T, (\mathbf{w}_{sa2})^T, (\mathbf{w}_{sa3})^T \end{bmatrix}^T$$

is the process noise vector. $\mathbf{\Gamma}_k$ is the coefficient matrix of process noise vector. $\mathbf{Z}_k$ is the measurement vector as introduced in Subsection III-C and III-D. $\mathbf{v}_k$ is the measurement noise vector. $f()$ and $h()$ are nonlinear functions.

As widely known, EKF performs the estimate of the state vector through time update and measurement update. No further details about EKF will be provided here due to space limitations.

IV. Practical Mechanisms to Realize Smooth Transitions

This research deployed kinematic trajectory model as the core of DKF system model. As can be seen from the discrete system model in Subsection III-B, the jerk vector in acceleration model describes transitions between alternative kinematic processes. In order to avoid large calculation, the jerk vector is disposed as process noise in Subsection III-E, so that the less complex kinematic model cannot realize smooth transitions between alternative kinematic models. On the premise of few additional calculations, practical detection rules will be developed to realize switches between

different kinematic models instead of establishing a complex kinematic model. The proposed practical mechanism utilizes the changes of linear and circular velocities and accelerations together with the changes of system attitudes.

This paper proposed the detection rules for significant system maneuvers by utilizing the raw outputs of center IMU, i.e. specific forces from accelerometers. Specifically, the specific force difference between this moment and the last is used to determine whether a switch occurs.

$$f^b_{ibx-imu1}(k) - f^b_{ibx-imu1}(k-1) < \sigma_1 \tag{40}$$

$$f^b_{iby-imu1}(k) - f^b_{iby-imu1}(k-1) < \sigma_2 \tag{41}$$

wherein, $f^b_{ibx-imu1}$, $f^b_{iby-imu1}$ are the specific forces of center IMU on the x axis and y axis respectively. σ_1, σ_2 could be set according to practical needs.

Only when accurate accelerations are obtained can relatively accurate velocities and positions be calculated. Additionally, the acceleration can be divided into tangential acceleration and normal acceleration by dynamics, which would simplify the analysis process sharply. As for linear and circular motion, different solutions are given as follows.

A. Mechanism to Realize Smooth Transitions for Linear Motion

For linear motion, the changes of tangential acceleration a^b_{nby} can not be reflected from the attitudes of vehicle with subtle variances. Considering the systematic errors of these multiple IMUs, e.g. the biases and scale factor errors of gyroscopes and accelerometers, were individually modeled in Kalman filter, so that they could be updated with filtering updates. Moreover, this research utilized all of the measurements, inclusive of the ones from IMUs. The specific force on the travel axis (y axis) of center IMU indicates acceleration in the direction of travel. Therefore, the specific force on the travel axis with correction could be considered as an alternative of tangential acceleration. The tangential acceleration a^b_{nby} can be updated as follows

$$\begin{aligned} a^b_{nby}(k{+}1) = {} & \tfrac{f^b_{iby-imu1}(k)-b_{a1y}(k)}{1+s_{a1y}(k)} - \sin(P(k)) \cdot g_0 \cdot \\ & (1 + 0.0052884 \cdot \sin^2(\varphi(k)) - 0.0000059 \cdot \sin^2(2\varphi(k))) \end{aligned} \tag{42}$$

wherein, $f^b_{iby-imu1}$ is the specific force output of center IMU on the y axis. g_0 is the gravitational acceleration on the equatorial sea level. Other parameters have been introduced before.

Obviously, the estimation accuracy for accelerometer biases and scale factors influences the effectiveness of the solution. The simulation results show that accelerometer biases and scale factors estimation accuracy obviously decreases during circular motion, which leads to another solution to be needed for this process.

B. Mechanism to Realize Smooth Transitions for Circular Motion

For circular motion, normal acceleration a^b_{nbx} is the main target to be discussed. According to system dynamics and kinematics, the attitudes will change with the changes of linear and circular velocities and accelerations. Actually, to ground based vehicle, only the change of direction angle is the most obvious, as follows

$$\psi(k{+}1) = \psi(k) + \frac{a^b_{nbx}(k)}{v^b_{nby}(k)} \cdot \Delta t \tag{43}$$

wherein, ψ is the direction angle. $\Delta t = t_{k+1} - t_k$ is the time interval. v^b_{nby} is the linear velocity. In discrete system model, attitude model is independent of acceleration. Beyond that, the linear speed is constant in uniform circular motion. Therefore, normal acceleration a^b_{nbx} can be updated depending on the direction angle, as follows

$$a^b_{nbx}(k) = \frac{\psi(k{+}1) - \psi(k)}{\Delta t} \cdot v^b_{nby}(k) \tag{44}$$

As can be seen from (44), this model will be more accurate for circular motion with a constant magnitude of v^b_{nby}, such as uniform circular motion.

TABLE I
THE TRANSITIONS DURING ONE-MINUTE TRACK

Time Interval	Acceleration	Travel Distance
0-10s	$a_n = 0, a_t = 2\mathrm{m/s}^2$	S=100m
10-50s	$a_n = 0, a_t = 0$	S=800m
50-55s	$a_n = 0, a_t = -3\mathrm{m/s}^2$	S=62.5m
55-57s	$a_n = -5\pi/4\mathrm{m/s}^2, a_t = 0$	S=10m
57-60s	$a_n = 0, a_t = 0$	S=15m

V. SIMULATIONS AND RESULTS

The unconventional integrated navigation strategy will be applied to process the navigation information collected by GPS and multiple low-cost IMUs integrated navigation system on a ground based vehicle. In this paper, all tests are under full physical simulation. The trajectory simulation of the vehicle was designed in this research as a temporary replacement of real body. Besides, the real-time raw outputs of three IMUs and GPS were simulated on practical basis. In order to imitate the output from real sensor, several groups of random numbers were generated through a series of procedures, not generated by utilizing functional instructions that come with Matlab. Here no more details about this part will be introduced due to the space limit. The IMU data were collected at 100Hz (angular rate: bias stability $\approx 10.0^\circ/\mathrm{h}$, angle random walk $\approx 4.5^\circ/\sqrt{\mathrm{hr}}$; specific force: bias stability $\approx$ 0.1mg, velocity random walk $\approx 1.0\mathrm{m/s}/\sqrt{\mathrm{hr}}$) and the GPS data were acquired at 1Hz. The GPS simulation was based on a navigation message file. One-minute track with a plurality of transitions was selected to demonstrate the practicability of the proposed method, see Table I for details.

Fig. 4 - Fig. 7 show the solution accuracies for kinematic trajectory parameters and attitude under the practical mechanisms (PMs). The accuracy of 3D position solution is under $20\mathrm{m}$. The overall accuracies for velocity state vector in east, north and up directions are approximately $\pm 0.5\mathrm{m/s}$, $0 \sim 0.4\mathrm{m/s}$ and $\pm 0.5\mathrm{m/s}$, respectively. The accuracy for acceleration state vector in up direction is always within $0.05\mathrm{m/s}^2$. The accuracies for acceleration state vector in east and north directions are also relatively high, especially for linear motion. The errors of acceleration in three directions are slightly larger during the turn (55-57s) due to attitude

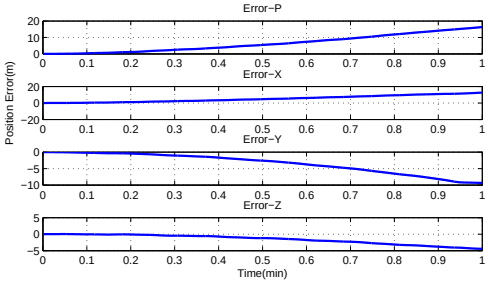

Fig. 4. 3D Position Solution Accuracy in S_e Using PMs

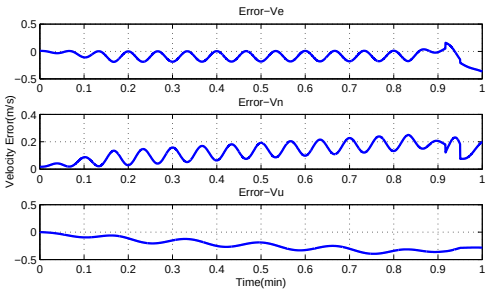

Fig. 5. 3D Velocity Solution Accuracy in S_n Using PMs

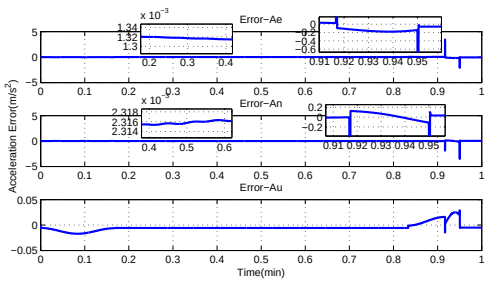

Fig. 6. 3D Acceleration Solution Accuracy in S_n Using PMs

accuracy, though the overall accuracy for acceleration is acceptable. The estimation errors of attitude (roll, pitch and heading) are around $\pm 0.5^\circ$, $\pm 0.5^\circ$ and $\pm 1^\circ$, correspondingly.

Fig. 8 - Fig. 10 show the solution accuracies for kinematic trajectory parameters with and without the PMs. It can be seen clearly that the divergent growth of position and velocity errors could be well suppressed using the practical mechanisms. For acceleration error, the accumulated acceleration error caused by switches between different kinematic models could be effectively avoided by the practical mechanisms.

Furthermore, the estimates for three IMUs systematic errors, i.e. three-axis biases and scale factor errors of gyroscopes and accelerometers, are illustrated in Fig. 11 - Fig. 14. Remarkably, almost all the estimations of system errors deviate from the relative steady values after 55s. That is why different solutions are selected for the linear and circular motion.

Generally, the navigation parameters during accelerated, uniform and circular processes could be estimated within acceptable ranges using the unconventional multi-sensor integration strategy with the proposed PMs. Moreover, all the error curves show the gradual upward trend, which is due to the simplification of system model, but has no significant effect on navigation accuracy in a short period.

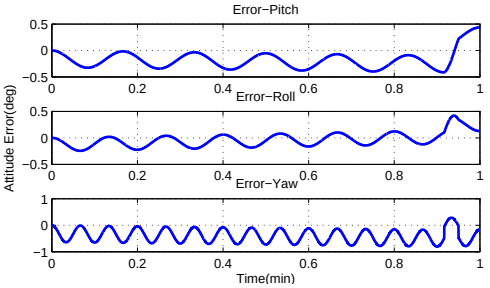

Fig. 7. Attitude Solution Accuracy Using PMs

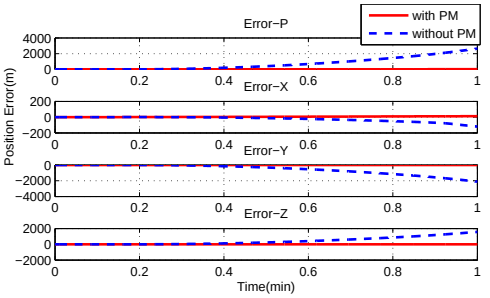

Fig. 8. 3D Position Solution Accuracy Comparisons with or without PMs

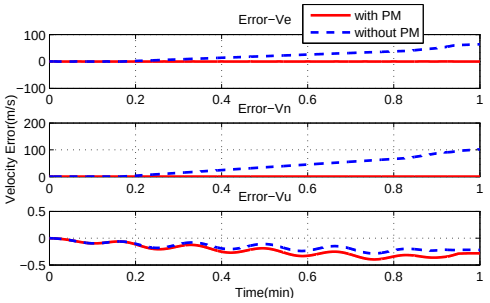

Fig. 9. 3D Velocity Solution Accuracy Comparisons with or without PMs

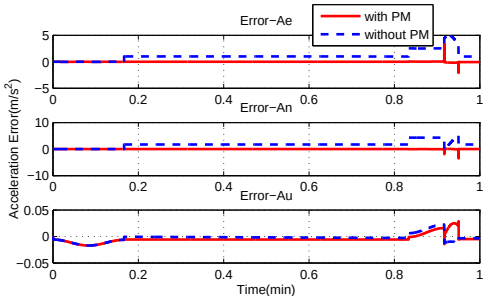

Fig. 10. 3D Acceleration Solution Accuracy Comparisons with or without PMs

VI. Conclusion

This research applied the novel multi-sensor integration strategy based on kinematic trajectory model to integrate GPS receiver and three low-cost IMUs. The improved and enhanced part is the proposed practical mechanisms to realize smooth transitions between different motion statuses so that this integration strategy would be widely applied to continuous dynamic switching processes. The test results from the simulation of a ground based vehicle have demonstrated the practicability of the proposed practical mechanisms. The next task would be developing an algorithm of variance component estimation, so that the variances for process and

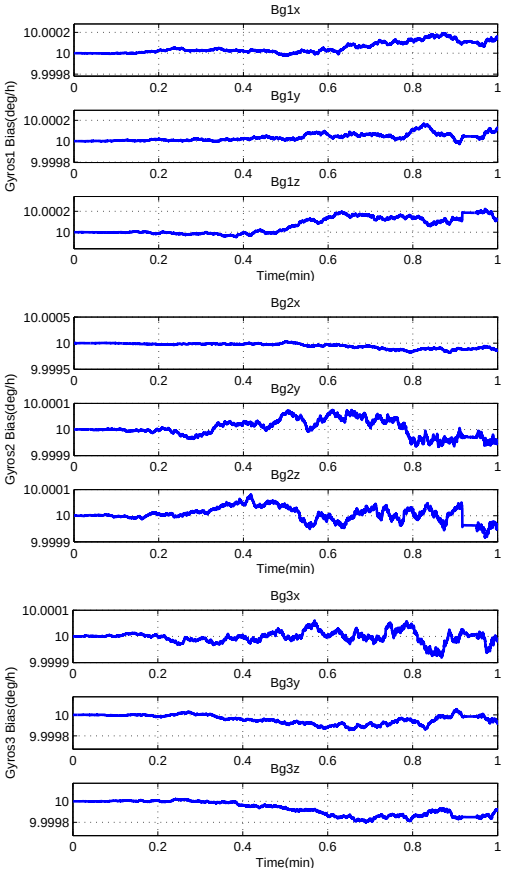

Fig. 11. Multi-gyroscope Bias Estimation

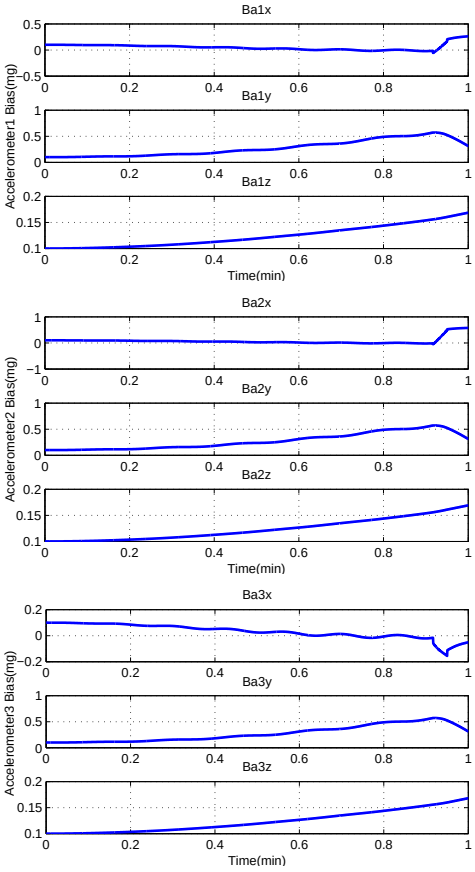

Fig. 13. Multi-accelerometer Bias Estimation

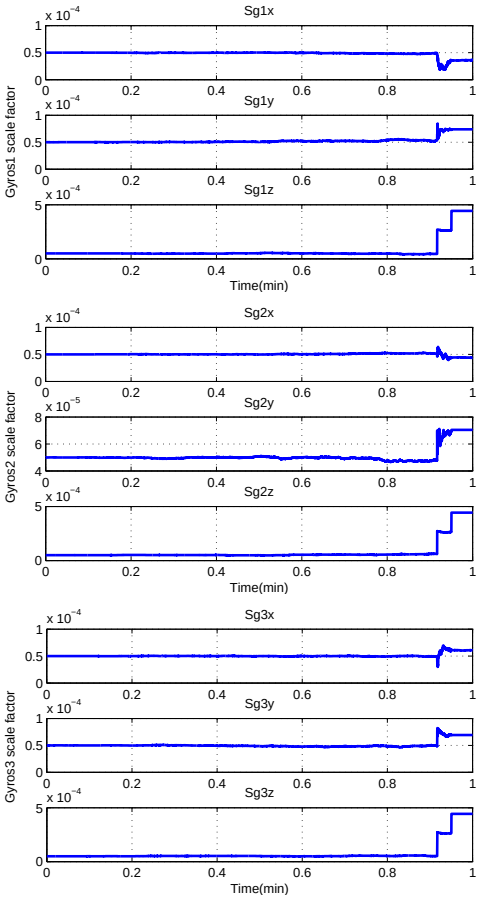

Fig. 12. Multi-gyroscope Scale Factor Estimation

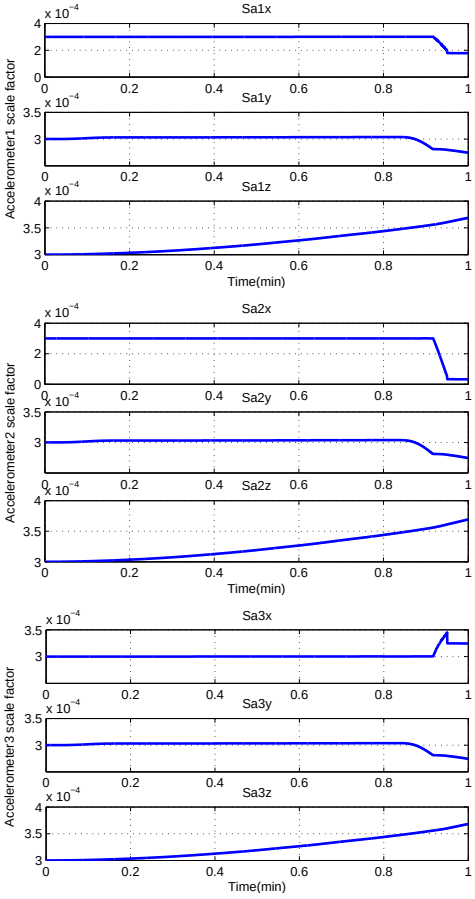

Fig. 14. Multi-accelerometer Scale Factor Estimation

measurement noises could be updated in Kalman filter to produce reliable result and restrain divergence.

REFERENCES

[1] I. Skog, J. O. Nilsson and P. Handel, "An Open-source Multi Inertial Measurement Unit (MIMU) Platform[C]," in *International Symposium on Inertial Sensors and Systems IEEE*, pp. 1-4, 2014.

[2] C. Y. Jiang, L. Xue and H. L. Chang, "Signal Processing of MEMS Gyroscope Arrays to Improve Accuracy Using a 1st Order Markov for Rate Signal Modeling," *Sensors*, vol. 12, no. 2, pp. 1720-1737, 2012.

[3] D. Titterton and J. Weston, "Strapdown Inertial Navigation Technology," *Aerospace & Electronic Systems Magazine IEEE*, vol. 20, no. 7, pp. 33-34, 2004.

[4] C. Jekeli, "Inertial Navigation Systems with Geodetic Applications[M]," *Walter de Gruyter*, 2001.

[5] M. Eldiasty and S. Pagiatakis, "A Rigorous Temperature-Dependent Stochastic Modelling and Testing for MEMS-Based Inertial Sensor Errors," *Sensors*, vol. 9, no. 11, pp. 8473, 2009.

[6] G. D. Pasquale and A. Somà, "Reliability Testing Procedure for MEMS IMUs Applied to Vibrating Environments," *Sensors*, vol. 10, no. 1, pp. 456-474, 2010.

[7] J. G. Wang, K. Qian and B. Hu, "Novel Integration Strategy for GNSS-Aided Inertial Integrated Navigation," *Geomatica*, vol. 69, no. 2, pp. 217-230, 2015.

[8] J. G. Wang, K. Qian and B. Hu, "An Unconventional Full Tightly-Coupled Multi-Sensor Integration for Kinematic Positioning and Navigation[C]," in *China Satellite Navigation Conference (CSNC) 2015 Proceedings: Volume III. Springer Berlin Heidelberg*, pp. 753-765, 2015.

[9] K. Qian, J. G. Wang and B. Hu, "A posteriori estimation of stochastic model for multi-sensor integrated inertial kinematic positioning and navigation on basis of variance component estimation," *The Journal of Global Positioning Systems*, vol. 14, no. 1, pp. 5, 2016.

[10] F. Srairi, L. Saidi, F. Djeffal and M. Meguellati, "Modeling, Control and Optimization of a New Swimming Microrobot Design," *Engineering Letters*, vol. 24, no. 1, pp. 106-112, 2016.

[11] Z. Qi and Q. Y. Wang, "Error Analysis and the Development of an Error Mitigation Approach for Use in the Rotation Fiber Optic Gyro Inertial Navigation System," *Engineering Letters*, vol. 21, no. 4, pp. 203-211, 2013.

[12] J. B. Bancroft and G. Lachapelle, "Data Fusion Algorithms for Multiple Inertial Measurement Units," *Sensors*, vol. 11, no. 7, pp. 6771-6798, 2011.

[13] L. Xue, C. Y. Jiang and H. L. Chang, "A novel Kalman filter for combining outputs of MEMS gyroscope array," *Measurement*, vol. 45, no. 4, pp. 745-754, 2012.

[14] R. Munguła, "A GPS-aided Inertial Navigation System in Direct Configuration," *Journal of Applied Research & Technology*, vol. 12, no. 4, pp. 803-814, 2014.

[15] X. Song, X. Li, W. G. Zhang and W. C. Tang, "RFID Application for Vehicle Fusion Positioning in Completely GPS-denied Environments," *Engineering Letters*, vol. 24, no. 1, pp. 19-23, 2016.